

PREDICTED PERFORMANCE OF AN X-RAY NAVIGATION SYSTEM FOR FUTURE DEEP SPACE AND LUNAR MISSIONS

Joel Getchius*, Anne Long†, Mitra Farahmand†, Luke Winternitz‡, Munther A. Hassouneh‡, and Jason W. Mitchell‡

In November 2017, the NASA Goddard Space Flight Center Station Explorer for X-ray Timing and Navigation Technology experiment successfully demonstrated the feasibility of X-ray Pulsar Navigation (XNAV) as part of the Neutron Star Interior Composition Explorer mission, which is an X-ray Astrophysics Mission of Opportunity currently operating onboard the International Space Station. XNAV provides a GPS-like, absolute autonomous navigation and timing capability available anywhere in the Solar System and beyond. While the most significant benefits of XNAV are expected to come in support of very deep-space missions, the absolute autonomous navigation and timing capability also has utility for inner Solar System missions where increased autonomy or backup navigation and timing services are required, e.g., address loss of communication scenarios.

The NASA commitment to develop a Gateway to support exploration of the Moon and eventually Mars, as well as current and future robotic missions such as James Webb Space Telescope and New Horizons, certainly will tax the existing ground based infrastructure in terms of availability. Therefore, an extended look at the feasibility and potential performance of XNAV for comparable missions is warranted. In this paper, we briefly review the XNAV concept and present case studies of its utility and performance for a Gateway orbit, Sun-Earth libration orbit, and a deep space transit trajectory.

INTRODUCTION

While the concept of X-ray Pulsar Navigation (XNAV) has been discussed for decades,¹ only since November 2017 has a real-time, in-flight demonstration of the technology been achieved. The Station Explorer for X-ray Timing and Navigation Technology (SEXTANT) experiment is a subset of the larger Neutron Star Interior Composition Explorer (NICER) mission flown on the International Space Station (ISS). Recent results from these efforts have illustrated the successful use of Millisecond Pulsars (MSP), i.e., rapidly rotating neutron stars with emissions in the X-Ray spectrum, to resolve timing, position, and velocity of the ISS in low Earth orbit.^{2,3} Specific details on the real-time performance and navigation accuracies achieved can be found in the cited references.

NICER/SEXTANT generates pulse phase and frequency measurements by tracking MSPs using 56 co-aligned X-ray concentrator optics of which 52 are currently operating on-orbit. Also available is the option to use timing synchronization via the Global

* Omitron, Inc., Beltsville, MD 20771, USA.

† a.i. solutions, Inc., Lanham, MD 20706, USA.

‡ NASA Goddard Space Flight Center, Greenbelt, MD 20771, USA.

Positioning System, which allows for experiments in time determination or position and velocity determination using GPS quality clocks. These measurements are processed in an extended Kalman filter (EKF) provided by the Goddard Space Flight Center (GSFC) Goddard Enhanced Onboard Navigation System (GEONS).

In addition to demonstrating real-time performance and feasibility, the results of the NICER/SEXTANT experiment have been employed to improve the XNAV measurement models in a ground-based GEONS-inclusive simulation at GSFC. With the improved models and the ability to simulate trajectories anywhere in the solar system, it is worthwhile to examine the predicted navigation performance of XNAV for several mission types:

- A Near-Rectilinear Halo Orbit (NRHO) that is a candidate for NASA's Gateway
- A Sun-Earth Libration Point 2 (L2) orbit similar to that of telescope missions such as James Webb Space Telescope (JWST) and Wide Field Infrared Survey Telescope (WFIRST)
- A deep-space interplanetary cruise trajectory such as performed by the New Horizons spacecraft

In this paper, after describing our simulation capabilities, we present predicted XNAV performance using a NICER/SEXTANT-like sensor for each of these mission profiles as well as a brief comparison to the navigation performance that can be achieved by processing range and Doppler measurements from ground station tracking systems. The collecting area of the modeled XNAV sensor, i.e., the number of NICER concentrators, is also traded for each mission profile. We conclude with a brief discussion of conclusions.

GEONS GROUND MATLAB SIMULATION

GEONS is a high Technology Readiness Level (TRL), flight-proven navigation software package developed at GSFC.⁴ Past and present flight heritage includes the Magnetospheric Multiscale Mission, Global Precipitation Mission, and SEXTANT. In addition, a GEONS Ground MATLAB Simulator (GGMS) has been developed to perform navigation related analyses. A functional diagram of GGMS appears in Figure 1. The GGMS consists of custom MATLAB simulation scripts that control the simulation and data analysis processing, the GEONS MATLAB API that provides the interface between the MATLAB simulation and the GEONS flight software library, and the GEONS flight software methods that are used to simulate measurements, process measurements, and propagate and update the state and covariance. The object-oriented structure of the GEONS code base allows for this simulation architecture. As an example of the simulation procedure, consider the steps performed by the MATLAB simulation driver to simulate and process an XNAV measurement:

1. Based on an observation schedule built with custom MATLAB code, a call is made to GEONS to simulate an error-free set of XNAV measurements using the truth trajectory
2. The error-free XNAV measurements are retrieved by the MATLAB driver and degraded with noise and bias, as specified.
3. The degraded XNAV measurements are returned to GEONS along with the navigation state and processed by the GEONS EKF.
4. The difference between the GEONS state estimates and truth trajectory are computed and plotted.

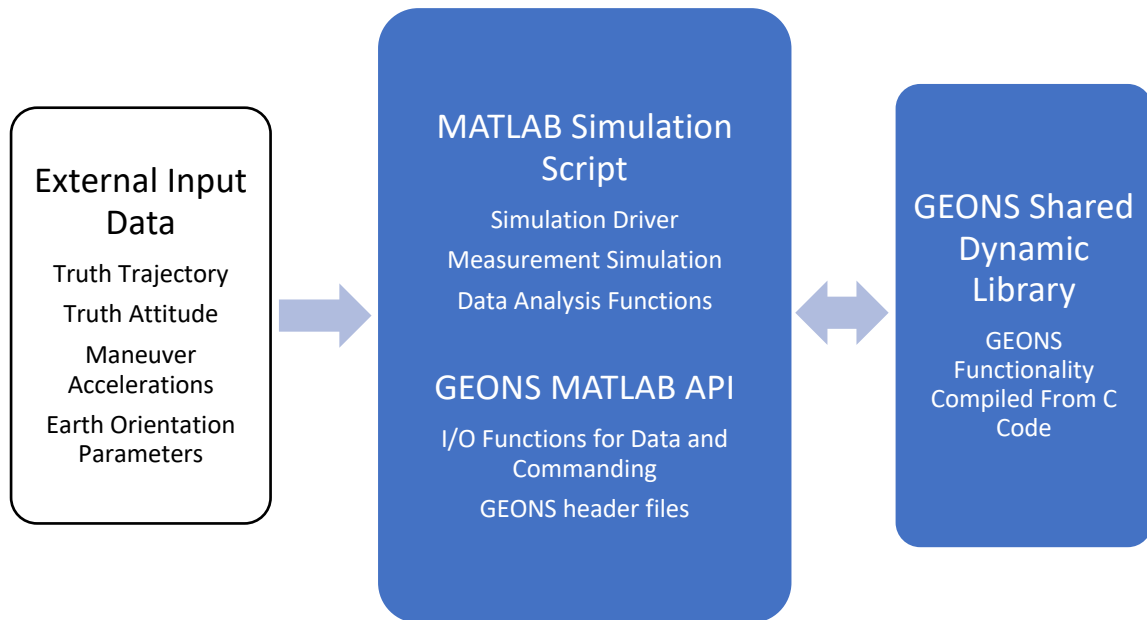


Figure 1: Overview of the GGMS and its relation to the GEONS software library.

The GGMS architecture provides maximum flexibility to the analyst, while leveraging the high TRL and verified mathematical models from GEONS. Sufficient flexibility is built into the GGMS to allow for the use of ephemerides for truth versus an option to propagate a truth trajectory, maneuver ingestion, data preservation and analysis, and a Monte Carlo functionality.

Results from single runs are presented for the cases presented in this study. While not statistically robust, these cases offer insight to the potential level of performance, as well some insight to sensitivities. The mission profiles examined process simulated XNAV measurements in the GEONS EKF. The XNAV results are compared to the performance expected from processing ground-based tracking measurements.

XNAV Measurement Model

Similar to GPS, the relative geometry of the observed pulsars is an important consideration in the navigation performance. The five pulsars (B1821–24, B1937+21, J0218+4232, J0030+0451, and J0437–4715) used in this study provide an excellent geometric distribution. For convenience, spacecraft structural occultations and occultations by the Sun, Moon, and other bodies were ignored in determination of pulsar visibility. Future work includes updating the GGMS with these constraints and evaluating their impact to navigation performance and operations.

Per Reference 3, the pulsar pulse phase measurement, $\phi(t)$, can be expressed by Equation (1).

$$\phi(t) = \phi_o(t^*(t)) \quad (1)$$

Where $t^*(t) = t - \frac{b(t)}{c} + \frac{\hat{\mathbf{n}} \cdot \mathbf{x}(t)}{c}$ and is the time of arrival of the pulsar wave front at the reference observatory, $\phi_o(t^*(t))$ is the pulsar phase at a specified reference observatory, t is the time of arrival at the detector, $b(t)$ is the spacecraft clock bias in meters, $\hat{\mathbf{n}}$ is the unit vector in the direction of the pulsar in the inertial frame, $\mathbf{x}(t)$ is the position of the spacecraft in the inertial frame, and c is the speed of light.

The derivative of Equation (1) yields the formula for the frequency measurement:

$$\frac{d\phi(t)}{dt} = \dot{\phi}_o(t^*(t)) \times \left[1 - \frac{\dot{b}(t)}{c} + \frac{\hat{\mathbf{n}} \cdot \mathbf{v}(t)}{c} \right] \quad (2)$$

where $\dot{\phi}_o(t^*(t))$ is the pulsar reference frequency at a specified reference observatory, $\dot{b}(t)$ is the clock rate in meters per second, and $\mathbf{v}(t)$ is the spacecraft velocity vector. Note that $\frac{\dot{b}(t)}{c}$ is the correction to the reference frequency due to the time-bias rate and $\frac{\hat{\mathbf{n}} \cdot \mathbf{v}(t)}{c}$ is the Doppler shift due to the motion of the detector. Although both measurement formulations include parameterization of clock errors, the studies presented here ignore the contributions of clock errors and make no attempt to estimate clock parameters. Such an assumption of a “perfect” clock is consistent with an operational model where the spacecraft clock is comparable to the performance of an atomic clock or periodically resynched via ground range measurements. References 2 and 3 discuss clock bias and rate estimation during the SEXTANT experiment. Future work will examine clock bias and

* Note that the reference observatory is located at the geocenter in this study and the detector is located on the spacecraft.

rate estimation for the presented mission profiles. References 2 and 3 also provide a more nuanced discussion of the generation of the pulse phase and frequency measurements, along with issues associated with each measurement.

Since the XNAV measurements are formulated as pulse phase and frequency, a pulsar specific integration time is required for measurement construction. The integration times needed to provide accurate measurements are pulsar specific because of the varying frequencies and intensities of each pulsar. To simulate phase measurements with comparable accuracies, the integration time are scaled linearly with the number of concentrators. The integration time, Δt , is given by Equation (3).

$$\Delta t = \Delta t_o \frac{56}{n_c} \quad (3)$$

where Δt_o is the default integration time for the original NICER/SEXTANT 56 concentrator configuration and n_c is the number of concentrators simulated. Table 1 lists the default integration times per pulsar used in this analysis, which are based on the values used by NICER/SEXTANT.

Table 1: Per Pulsar Integration Time for the 56-Concentrator Configuration⁵

| Pulsar | Integration Time, Δt_o (s) |
|------------|------------------------------------|
| B1821–24 | 400 |
| B1937+21 | 900 |
| J0218+4232 | 1200 |
| J0030+0451 | 900 |
| J0437–4715 | 900 |

Experimental results from NICER/SEXTANT have shown the errors in the pulse phase measurement scale as $\frac{1}{\sqrt{\Delta t}}$ and for the frequency measurement as $\left(\frac{1}{\sqrt{\Delta t}}\right)^3$ (Reference 4).

Ground Station Measurement Model

To provide a means of comparison, the XNAV performance in the following simulations are compared to the results from navigation performance from simulated ground tracking. The GGMS can simulate standard 2-way range and Doppler measurements from any specified ground station. For these studies, Deep Space Network (DSN)-like performance and geometry is assumed from stations located at Canberra (Australia), White Sands (New Mexico), Goldstone (California), and Madrid (Spain). Specific ground tracking assumptions are discussed in each simulation scenario since the analysis attempted to recreate known ground station operations.

GATEWAY SIMULATION

The orbit studied for the Gateway is an Earth-Moon L2 Southern NRHO with an average periapsis altitude of approximately 1800 km, an apoapsis altitude of 68,000 km, and a period of about 6.5 days. This orbit exhibits a 9:2 resonance with the Moon's orbit. Figure 2 illustrates a candidate NRHO for Gateway.⁶ The current study uses a truth trajectory nearly identical to that studied in Reference 6.



Figure 2: Illustration of NRHO trajectory.*

When examining a space-station trajectory, two distinct classes of trajectories are possible: crewed and un-crewed. When crewed, spacecraft experience trajectory perturbations sources include waste water dumps, attitude correction perturbations due to increased angular momentum from high intensity operations, and crew exercise. These perturbations result in an increased cadence in orbit maintenance maneuvers and operations for momentum unloads. Note these perturbations are difficult to predict and model in a navigation filter and therefore degrade the navigation solution. In contrast, un-crewed operations tend to be relatively benign, with perturbations limited to physical mismodeling of the space environment or maneuver execution errors.

We examined the cases of quiescent un-crewed and crewed NRHO trajectories that employ XNAV and compared those results to ground tracking limited to 8 hours a day alternating from Goldstone, Madrid, and Canberra. Analysis of the accuracy of the ground tracking case is presented in a companion paper.⁷ Our initial covariance assumes the initial filter state was based on prior processing of sufficient ground tracking, GPS, or both and is reflective of uncertainties of 1 km (1σ) and 0.02 m/s (1σ) each axis. The orbit maintenance maneuvers are modeled in the filter with errors of 1% (1σ) of the planned ΔV s. The impact of the number of concentrators is assessed. Table 2 lists the dynamic models used in the truth trajectory and the GEONS onboard filter. In addition, the following disturbances are modeled in the crewed truth trajectory:⁶

* Illustration courtesy of Michael Volle, a.i. solutions, Inc. Generated using FreeFlyer™.

- CO₂ expulsion puffs of 8.3480E-04 m/s every 10 min
- Attitude deadbands of 2.0043E-05 m/s every 70 min
- Attitude slews of 6.9751E-04 m/s every 3.2 hours
- Wastewater dumps of 1.8840E-03 m/s every 3.0 hours

Table 2: Dynamic Models Used in Simulation

| | Truth Trajectory Simulation | GEONS Filter Propagation |
|---------------------------------|--|--|
| Planetary Ephemeris | JPL DE 430 | JPL DE421 |
| Pont Mass Gravity | Sun, Earth, Venus, Mars, Jupiter, Saturn | Sun, Earth, Venus, Mars, Jupiter, Saturn |
| Lunar Gravity Model | 30x30 GRAIL PRIM660 | 30x30 LP100K |
| Solar Radiation Pressure | Spherical 24000 kg, 80 m ² , C _R = 2.0 | Spherical 24000 kg, 80 m ² , C _R = 2.0 |
| Orbit Maintenance ΔVs | Planned | Planned + 1% (1σ) |

Figure 3 shows representative position errors for a 10-concentrator XNAV configuration for the un-crewed trajectory. Figure 4 show representative velocity errors for a 10 concentrator XNAV configuration for the un-crewed trajectory. The range position and LOS velocity errors are the errors along the line-of-sight (LOS) from the Earth to the spacecraft and lateral error is the root-sum-square of the errors perpendicular to the LOS. For all cases studied, large velocity errors (up to 1.0 m/s) occur at the periapsis crossings of the NRHO trajectory, where the velocity is 20 times larger than at apoapsis.

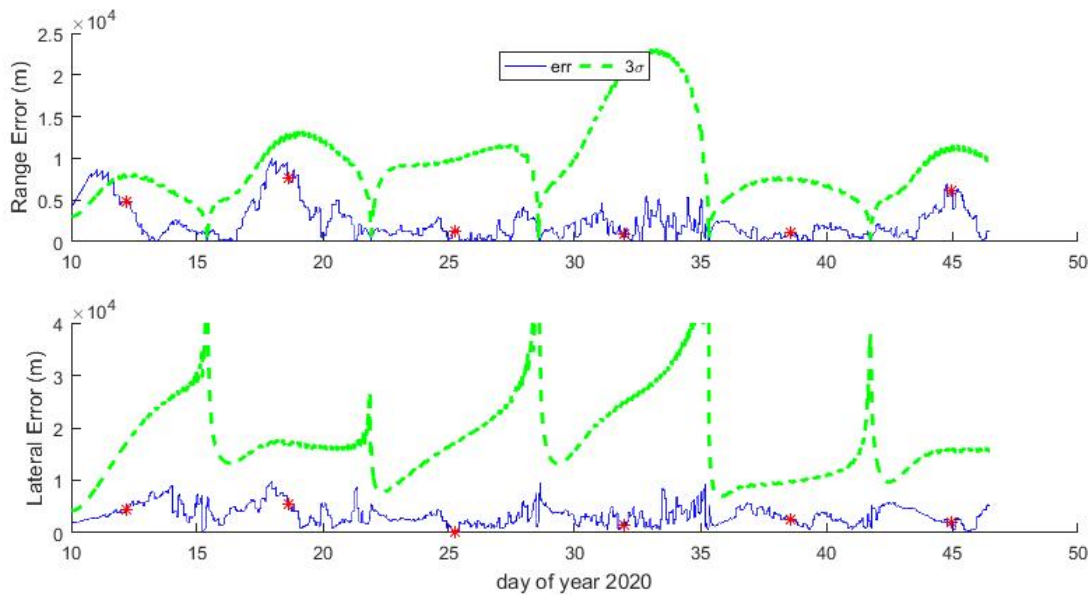


Figure 3: XNAV navigation position errors for 10-concentrator case in NRHO orbit for an uncrewed Gateway trajectory. Red asterisks indicate station keeping maneuver times and the green traces illustrate the 3σ position uncertainty computed from the covariance.

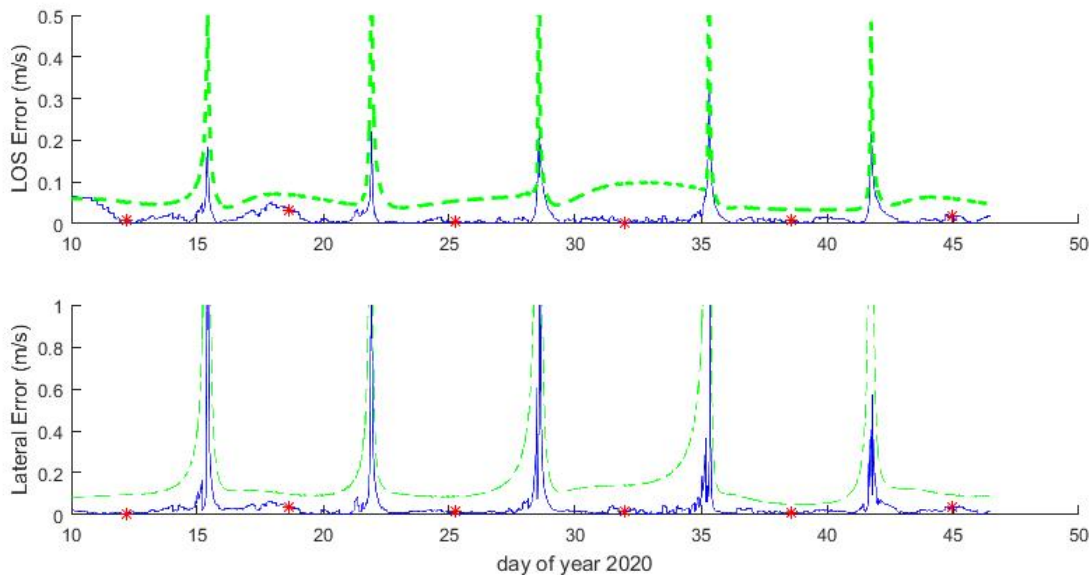


Figure 4: XNAV navigation velocity errors for 10-concentrator case in NRHO orbit for an uncrewed Gateway. Red asterisks indicate station keeping maneuver times and the green traces illustrate the 3σ velocity uncertainty computed from the covariance.

Figure 5 shows representative position errors for a 10-concentrator XNAV configuration for the *crewed* trajectory and Figure 6 shows representative velocity errors. The

performance is similar, although somewhat degraded, to that achieved on the un-crewed trajectory.

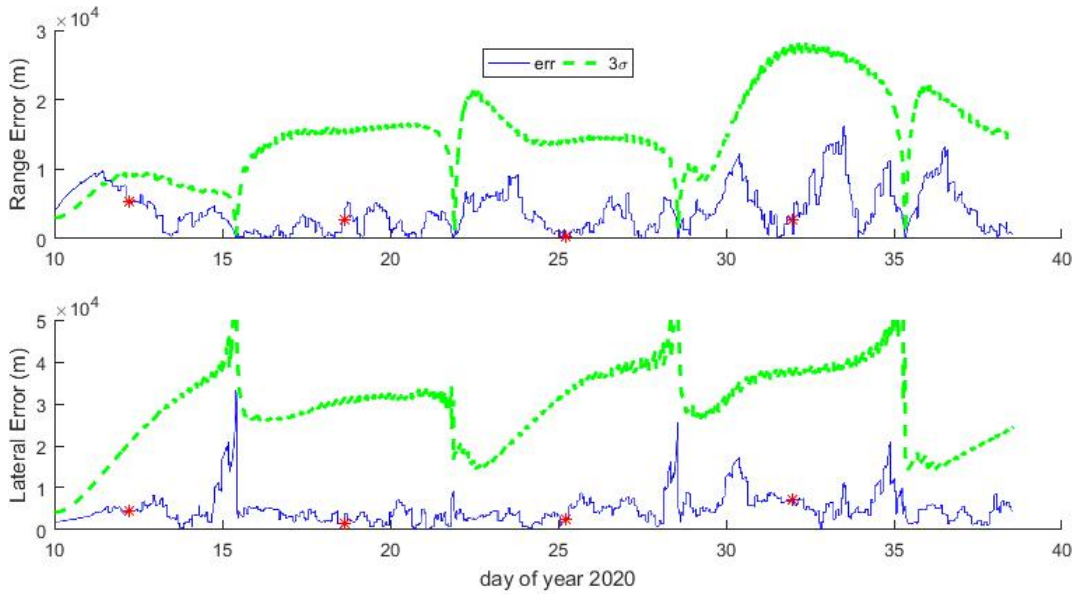


Figure 5: XNAV navigation position errors for 10-concentrator case in NRHO orbit for a crewed Gateway. Red asterisks indicate station keeping maneuver times (disturbances occur throughout) and the green traces illustrate the 3σ position uncertainty computed from the covariance.

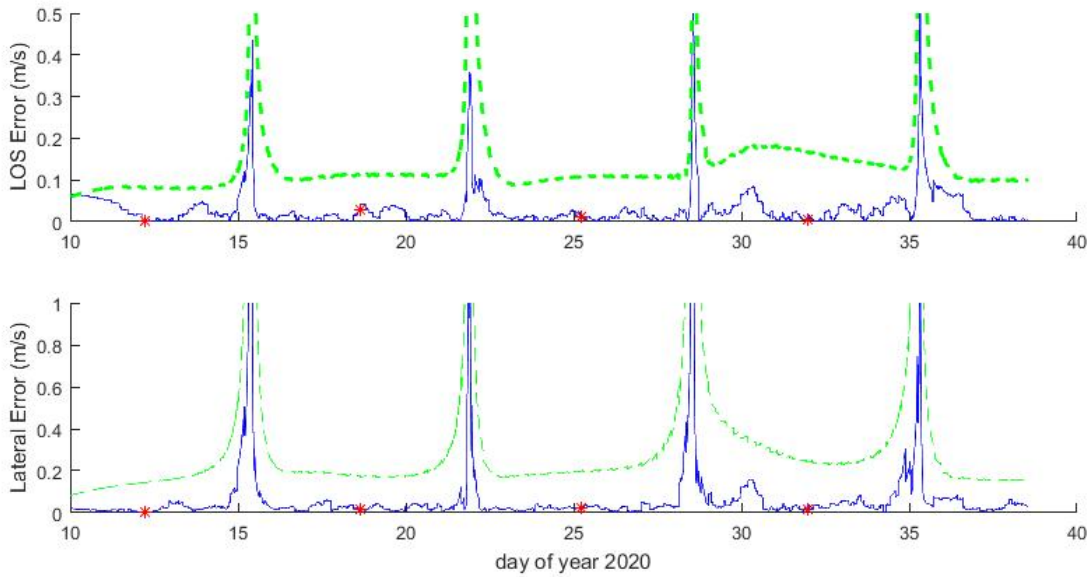


Figure 6: XNAV navigation velocity errors for 10-concentrator case in NRHO orbit for a crewed Gateway. Red asterisks indicate station keeping maneuver times (disturbances occur throughout) and the green traces illustrate the 3σ velocity uncertainty computed from the covariance.

After allowing for the initial filter transients to settle, Table 2 and Table 3 list the steady-state root-mean-square (RMS) errors for position and velocity as compared to the truth trajectory for the various XNAV concentrator configurations and the ground tracking case for the un-crewed and crewed trajectories, respectively.

Table 2: Steady-State RMS Position and Velocity Errors for Un-crewed NRHO

| | Average Measurement Frequency (min) | RMS Position Error (km) | RMS Velocity Error (m/s) |
|-----------------------|-------------------------------------|-------------------------|--------------------------|
| DSN | | 0.157 | 0.0035 |
| XNAV 56 Concentrators | 13 | 3.5 | 0.1331 |
| XNAV 10 Concentrators | 72 | 5.3 | 0.1631 |
| XNAV 4 Concentrators | 180 | 9.1 | 0.4101 |
| XNAV 1 Concentrators | 720 | 9.2 | 0.5814 |

Table 3: Steady State RMS Position and Velocity Errors for Crewed NRHO

| | Average Measurement Frequency (min) | RMS Position Error (km) | RMS Velocity Error (m/s) |
|-----------------------|-------------------------------------|-------------------------|--------------------------|
| DSN | | 2.73 | 0.052 |
| XNAV 56 Concentrators | 13 | 6.32 | 0.177 |
| XNAV 10 Concentrators | 72 | 7.89 | 0.275 |
| XNAV 4 Concentrators | 180 | 11.91 | 0.465 |
| XNAV 1 Concentrators | 720 | 16.45 | 0.977 |

At first glance, the results presented in Table 2 and Table 3 are not encouraging. Specifically, the velocity errors for the XNAV cases appear to be unacceptably high for use in planning for station-keeping maneuvers or momentum unloading. However, referring back to Figure 4 and Figure 6, large spikes in the velocity errors are limited to the periapsis crossing of the NRHO; whereas the orbit maintenance maneuvers occur at apoapsis. The relatively large integration times needed to construct accurate XNAV measurements using a small number of concentrators coupled with the rapidly changing geometry at periapsis is likely to be an issue for the NRHO trajectory, at least with an EKF formulation. It is worth examining in future work whether the effects of non-linearities at periapsis can be mitigated in an alternate filter formulation. Regardless, until rapid measurement formulation (i.e., small integration times) can be assured, XNAV best serves for portions of the orbit that do not have substantial changes in geometry short time frames. We note that this assertion does not necessarily mandate an improvement in sensor hardware; higher intensity pulsars would also decrease the integration time. For example, the

Crab pulsar (B0531+21) requires an integration time of 10 to 60 seconds. Regardless, these results demonstrate that XNAV could provide a backup capability for applications such as the pointing of a high gain antenna.

WFIRST SIMULATION

WFIRST is a proposed telescope mission to measure the effects of dark matter and dark energy. This mission profile includes a nominal halo orbit in the vicinity of the Sun-Earth L2 point with dimensions of 1.6 million kilometers in the long axis as viewed from ecliptic north in the rotating libration point frame (Figure 7) and a period of approximately 6 months. Figure 7 illustrates a representative trajectory in the rotating libration point frame.

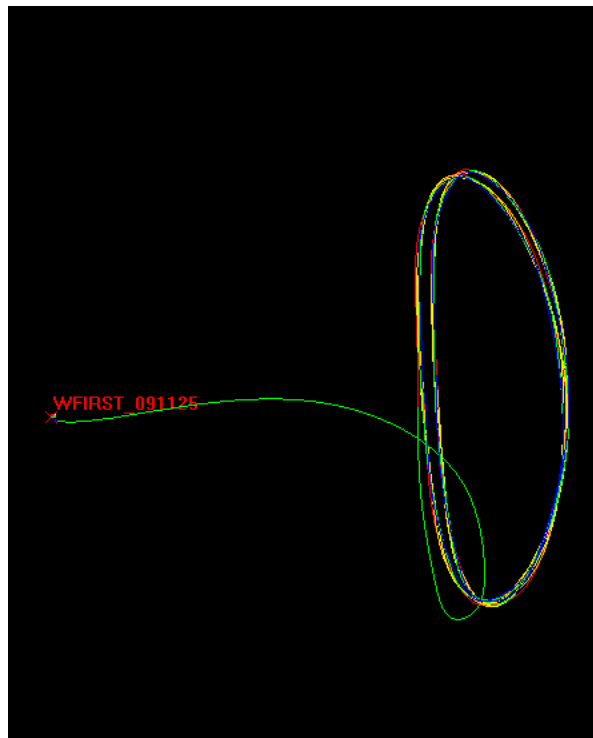


Figure 7: Illustration of WFIRST Sun-Earth L2 orbit and Earth-Moon transfer as observed from ecliptic North.

Because L2 is a marginally unstable equilibrium point, station-keeping maneuvers are required for orbital maintenance, i.e., approximately once every 4 weeks. The WFIRST trajectory design incorporates specific ground station coverage requirements to meet the demanding bandwidth needed for science data transfer. Additionally, as WFIRST is a telescope platform, stringent attitude requirements will require weekly momentum unloading of the spacecraft, resulting in a residual velocity change on the order of 13 mm/s per momentum unload. However, it is expected that these momentum unloads will occur at a known in time and be known in magnitude to within 0.5 mm/s. While the WFIRST orbit accuracy requirements are currently to-be-determined, it is expected that the definitive requirements will be on the order of the definitive requirements associated with the

JWST mission, which are 150 km (3σ) root-sum-square (RSS) position error and 2 cm/s (3σ) RSS velocity error.

Similar to the NRHO mission analysis, ground tracking results are compared to XNAV results for various concentrator configurations (56, 10, 4, and 1). In the case of WFIRST, the nominal daily ground tracking schedule consists of one hour of range and at least eight hours of Doppler from the White Sands ground station and one hour of range and Doppler from the Canberra ground station. This is representative of the expected ground tracking schedule on the WFIRST mission.

The GSFC Flight Dynamics Facility (FDF) produces a Mission Tracking Data Evaluation (MTDE) report for all spacecraft supported by the FDF.⁸ A product of the MTDE is the observed noise and bias for range and Doppler for each ground station that tracks these spacecraft. The range and Doppler measurement errors employed in this study were simulated using the statistics listed in Table 4. These statistics are based on recent FDF MTDE analysis of tracking measurement accuracy for the Deep Space Climate Observatory and the Solar and Heliospheric Observatory missions, which are in Sun-Earth L1 orbits at similar distance from the Earth as the WFIRST orbit. The truth trajectory includes momentum unloads every 200 hours with residual ΔV 's of 13.3 mm/s and station-keeping maneuvers every 25 days. The a priori covariance assumes state uncertainties of 30 km (1σ) and 2.2 cm/s (1σ) each axis, after initial insertion into the mission orbit. Representative errors and uncertainty in position for a 10-concentrator case are provided in Figure 8.

Table 4: Representative DSN Station Errors for Libration Point Missions (1σ)

| Station Location | Range Noise (m) | Range Bias (m) | Doppler Noise (m/s) | Doppler Bias (m/s) |
|------------------|-----------------|----------------|---------------------|--------------------|
| Canberra | 1.6 | 1.25 | 0.0005 | 0.0 |
| White Sands | 3.3 | 0.34 | 0.002 | 0.0 |

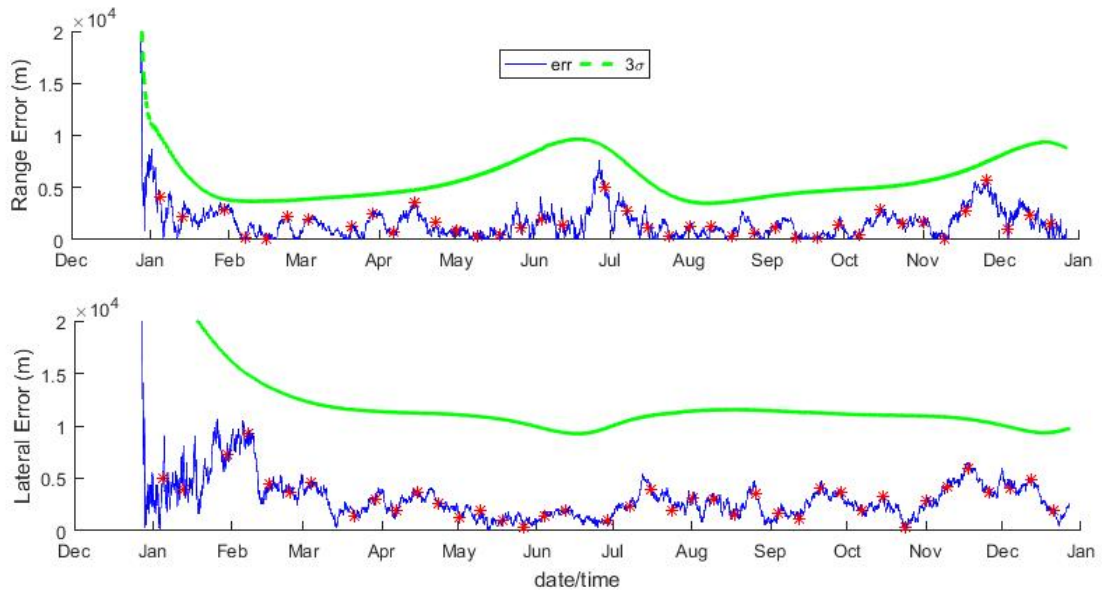


Figure 8: XNAV navigation position errors for 10-concentrator case in Sun-Earth L2 orbit for WFIRST. Red asterisks indicate station keeping maneuver times or momentum unloads and the green traces illustrate the 3σ position uncertainty computed from the covariance.

Figure 9 shows representative velocity errors and uncertainty results for WFIRST with a 10-concentrator XNAV configuration. As compared to the NRHO simulation, large spikes in the velocity errors are not present because the velocity is fairly consistent throughout the orbit. However, a seasonal signature appears due to changing relative geometry to the pulsars in use. It is expected that this may be mitigated with an increased pulsar catalog that provides more geometric diversity.

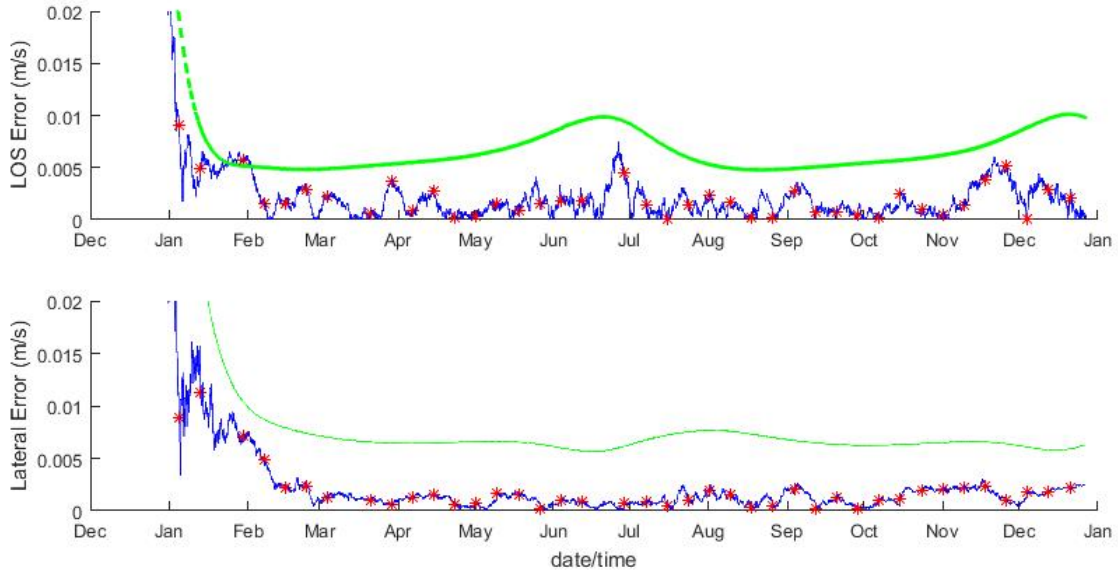


Figure 9: XNAV navigation velocity errors for 10-concentrator case in Sun-Earth L2 orbit for WFIRST. Red asterisks indicate station keeping maneuver times or momentum unloads and the green traces illustrate the 3σ velocity uncertainty computed from the covariance.

Table 5 lists the steady-state RMS errors for position and velocity as compared to the truth trajectory for the various XNAV concentrator configurations and the ground tracking case.

Table 5: Steady State RMS Position and Velocity Errors for WFIRST Utilizing Ground Tracking and XNAV

| | RMS Position Error (km) | RMS Velocity Error (m/s) |
|-----------------------|-------------------------|--------------------------|
| DSN | 1.5 | 0.0005 |
| XNAV 56 Concentrators | 1.7 | 0.0016 |
| XNAV 10 Concentrators | 3.4 | 0.0024 |
| XNAV 4 Concentrators | 4.5 | 0.0034 |
| XNAV 1 Concentrator | 7.2 | 0.0046 |

The slowly changing geometry of the WFIRST trajectory lends itself to a more robust and accurate XNAV solution for the larger integration times needed to construct the measurements in the cases with a lower number of concentrators. This effect is especially evident in the accuracy of the velocity components. Note that these results assume an accurate reconstruction of the station-keeping maneuvers as well as the momentum unloading events (less than 1 mm/s error). Such accuracies would be possible with

inflight calibration or the use of an onboard accelerometer. It is expected that the WFIRST station-keeping maneuvers will be relatively small (potentially as little as 6 mm/s) and therefore the navigation requirements to plan and execute the maneuver are on the order of 3 mm/s. Based on the results in Table 5, it is expected that a 56-concentrator or a 10-concentrator XNAV configuration would be sufficient to operate the WFIRST mission.

NEW HORIZONS SIMULATION

Launched in 2006, the New Horizons mission objectives include encountering and observing Pluto and other Kuper belt objects. This mission type requires a hyperbolic trajectory with a Solar System escape velocity. Figure 10 illustrates the New Horizons' trajectory with respect to the Earth.

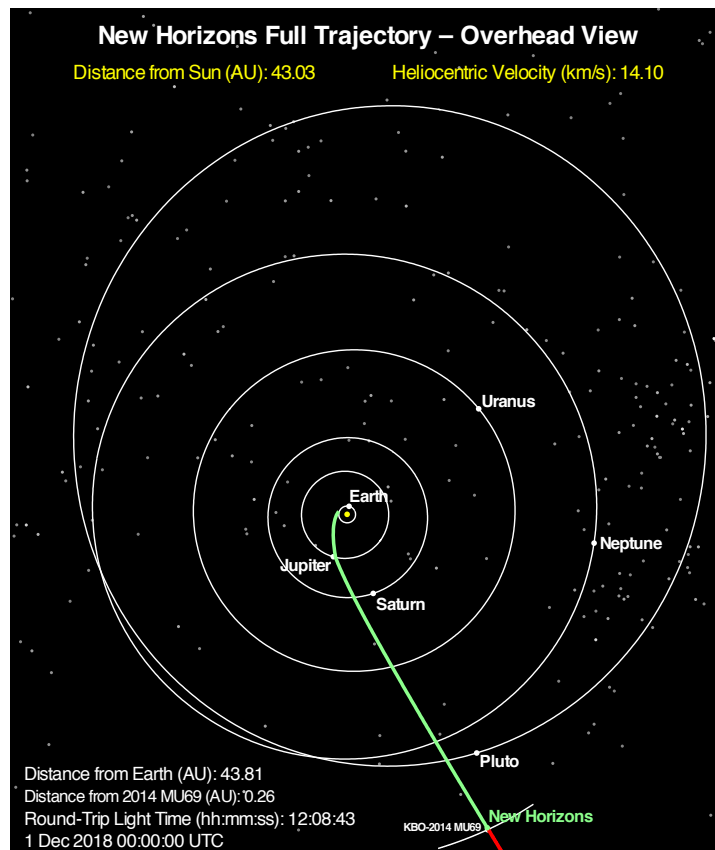


Figure 10: Illustration of New Horizons trajectory.*

Periodically, the New Horizons spacecraft enters into “hibernation” mode, where the spacecraft is in interplanetary cruise, not performing maneuvers (translational or attitude), and not performing science objectives, with only a keep-alive signal transmitted back to Earth. These quiescent periods of operations are advantageous to trade differing

* Image source: John Hopkins Applied Physics Laboratory website on New Horizons: <http://pluto.jhuapl.edu/Mission/Where-is-New-Horizons/index.php>

navigation architectures because errors in trajectory reconstruction are primarily caused by limitations to the navigation system.

One such hibernation period occurred near the Saturn orbit crossing for the month of June 2008. This swath of trajectory was selected to minimize the impacts of planetary body ephemerides uncertainty, which is especially a concern for outer Solar System bodies such as Neptune, Uranus, and Pluto. The ephemeris was obtained from JPL’s SPICE toolkit and the GGMS was used to recreate the one-month trajectory to within approximately 10 km of error (RSS).

During the periods of hibernation, the navigation plan for New Horizons includes sporadic radiometric measurements of 2-way range, 2-way Doppler, 3-way range, 3-way Doppler, or delta differential one-way range (Δ DOR).⁹ The capability of simulating and processing 3-way measurements or Δ DOR currently does not exist in GEONS. Therefore, continuous 2-way tracking from Canberra, Goldstone, and Madrid are simulated for this study. It is assumed that the overlapping contacts between these stations provides the equivalent geometric observation of the trajectory as 3-way tracking.¹⁰ It is *not* assumed that this tracking profile is equivalent to Δ DOR. Future work includes comparison of the XNAV results to those generated using Δ DOR. Table 6 lists the error model used in the simulated 2-way measurements.¹¹

Table 6: Representative DSN Station Errors (1σ)

| Station Location | Range Noise (m) | Range Bias (m) | Doppler Noise (m/s) | Doppler Bias (m/s) |
|------------------|-----------------|----------------|---------------------|--------------------|
| Canberra | 100.0 | 0.0 | 0.00011 | 0.0 |
| Goldstone | 100.0 | 0.0 | 0.00011 | 0.0 |
| Madrid | 100.0 | 0.0 | 0.00011 | 0.0 |

Once again, we trade a variety of XNAV concentrator configurations (56, 10, 4, and 1) and compare the results to navigation solutions generated via ground-based tracking. The initial covariance assumed state uncertainties of 10 km (1σ) and 1 m/s (1σ) for each inertial axis. Figure 11 shows representative position errors for a 10-concentrator XNAV system in interplanetary cruise. Figure 12 shows representative velocity errors for a 10-concentrator XNAV system in interplanetary cruise. The vertical axes of these plots are truncated to highlight the steady-state navigation performance.

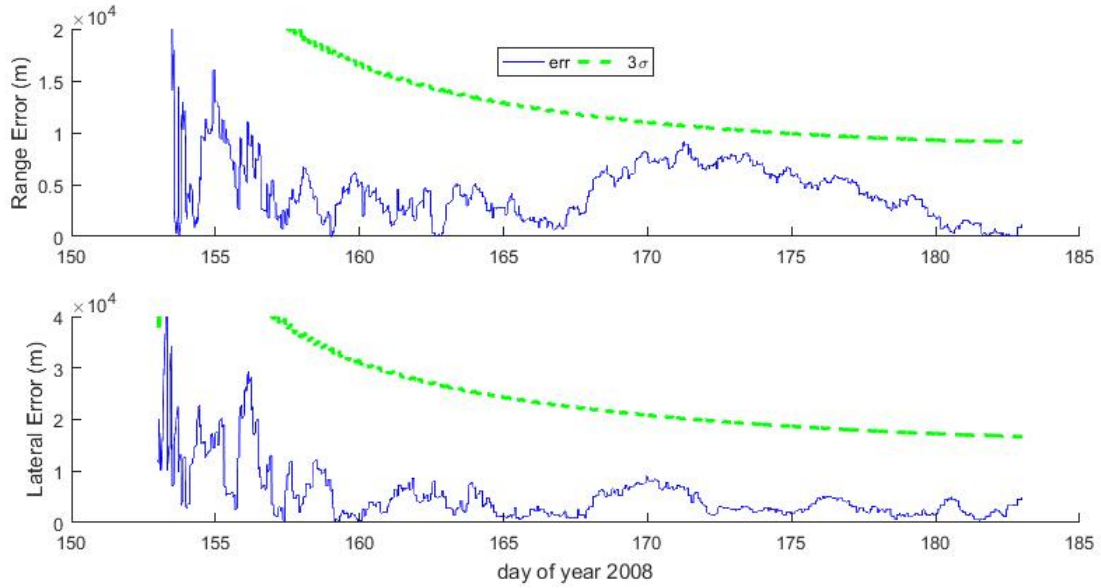


Figure 11: XNAV navigation position errors for 10-concentrator case in interplanetary cruise for New Horizons. Green traces illustrate the 3σ position uncertainty computed from the covariance.

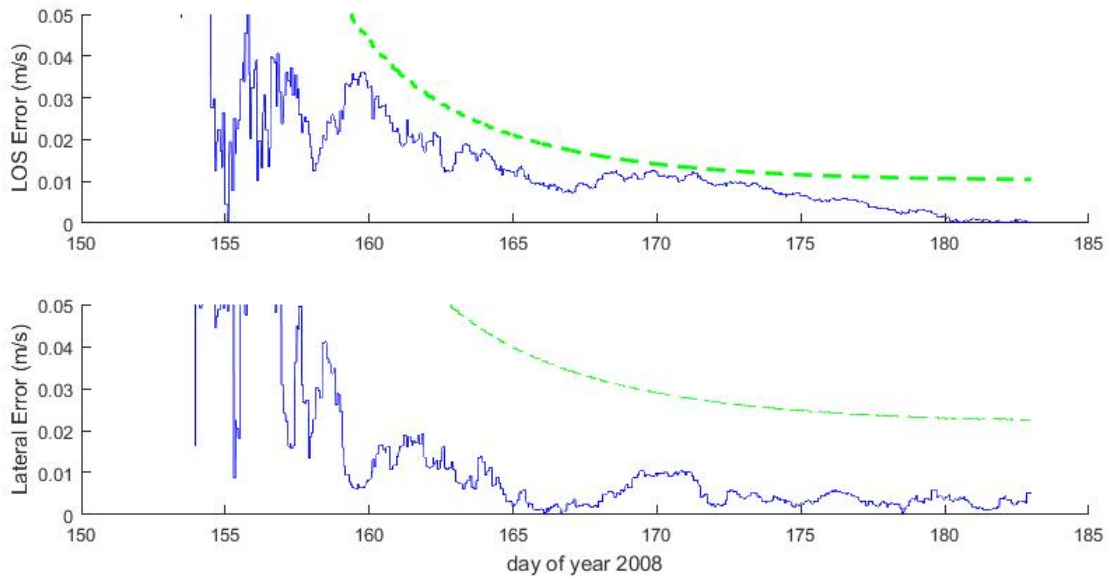


Figure 12: XNAV navigation velocity errors for 10-concentrator case in interplanetary cruise for New Horizons. Green traces illustrate the 3σ velocity uncertainty computed from the covariance.

Table 7 lists the steady-state RMS errors for position and velocity as compared to the truth trajectory for the various XNAV concentrator configurations and the ground tracking case. Here, we consider the system to be “steady-state” after two weeks of processing XNAV measurements.

Table 7: Steady-State RMS Position and Velocity Errors for New Horizons Utilizing Ground Tracking and XNAV.

| | RMS Position Error (km) | RMS Velocity Error (m/s) |
|-----------------------|-------------------------|--------------------------|
| DSN | 66.76 | 0.0508 |
| XNAV 56 Concentrators | 2.67 | 0.0038 |
| XNAV 10 Concentrators | 6.63 | 0.0090 |
| XNAV 4 Concentrators | 5.72 | 0.0111 |
| XNAV 1 Concentrator | 18.98 | 0.0125 |

The ground tracking results in Table 7 are pessimistic due to the use of overlapping tracking in place of Δ DOR measurements. Nearly the entire error with ground tracking is in the lateral direction; we expect that this error will significantly decrease with the addition of Δ DOR. The line of sight to Earth is resolved to less than 10 meters. Of issue is the large distance to the Earth and relatively small spacing between the ground stations, as the geometric observability degrades quickly in this mission profile. However, considering the navigation requirements for the Pluto flyby event range in B-plane components from 33 km to 66 km (1σ) and must be met with optical navigation augmenting radiometric navigation, the presented results appear reasonable. It is worth noting that these requirements are relative to Pluto where the largest error source is most certainly the location of Pluto itself and XNAV is an inertial navigation source – not a relative one. Note that, given the lack of literature on New Horizons navigation performance during the hibernation phases, peer review of these results is warranted and welcomed. Nevertheless, the degradation of navigation performance from ground tracking due to weak relative geometry is instructive to note.

In contrast, the geometric distribution of pulsars provides an excellent geometric fix. Furthermore, the slowly changing geometry of the trajectory segment studied is conducive for long integration times to support the formulation of the XNAV measurements. The limiting factor for XNAV system performance in this mission profile appears to be weak dynamical correlations in the filter propagation of the covariance that make resolving the position and velocity of the spacecraft difficult for any navigation architecture for spacecraft not in any gravity well. Improvement in XNAV performance could also be achieved by updating the pulsar reference frequency to either a Solar System Barycenter or reference trajectory frame of observation.

CONCLUSION

Leveraging the success of the NICER/SEXTANT XNAV demonstration, engineers at GSFC have enhanced their ability to simulate, predict, and analyze XNAV performance for a variety of mission scenarios. Here, we have presented representative performance

for a NRHO, Sun-Earth L2 orbit, and an interplanetary cruise mission profile. Sensitivity to integration times, and therefore concentrator configurations as well as trajectory geometry, have been demonstrated.

Although it still requires further development, XNAV, as demonstrated by NICER/SEXTANT and by this study, shows considerable promise to support future missions in their respective navigation trade spaces.

REFERENCES

- ¹ P. Buist, et al., “Overview of Pulsar Navigation: Past, Present and Future Trends.” *Journal of the Institute of Navigation*. Vol. 58, No. 2, 2011, pp. 153–164.
- ² J. Mitchell, et al., “SEXTANT X-RAY Pulsar Navigation Demonstration: Initial On-Orbit Results.” *AAS Guidance and Control Conference*, Univelt, San Diego, CA, 2018.
- ³ L. Winternitz et al., “SEXTANT X-RAY Pulsar Navigation Demonstration: Additional On-Orbit Results.” *15th International Conference on Space Operations*, 2018.
- ⁴ Goddard Space Flight Center Code 590, *Goddard Enhanced Onboard Navigation System (GEONS) Mathematical Specifications, Release 3.0*, A. Long, January 2019
- ⁵ A. Long and M. Farahmand, “Onboard Orbit Determination Analysis Using XNAV Measurements.” *NASA Internal Technical Memo*, FDSS-II-32-0002, 2018.
- ⁶ M. Volle and D. Davis, “Examining the Feasibility of Relative-Only Navigation for Crewed Missions to Near Rectilinear Halo Orbits.” *AAS Astrodynamics Specialist Conference*, Snowbird, UT, 2018.
- ⁷ L. Winternitz, et al., “GPS-Based Autonomous Navigation Study for the Lunar Gateway.” *AAS Guidance and Control Conference*, Breckenridge, CO, 2019.
- ⁸ B. Sease, et al., “Preliminary Analysis of Ground-Based Orbit Determination Accuracy for the Wide Field Infrared Survey Telescope (WFIRST).” *AAS/AIAA Astrodynamics Specialist Conference*, Stevenson, WA, 2017.
- ⁹ J. Miller, et al., “New Horizons Navigation to Pluto.” *AAS Guidance and Control Conference*, Breckenridge, CO, 2008.
- ¹⁰ T. Lee, et al., “Navigating the Return Trip from the Moon Using Earth-Based Ground Tracking and GPS.” *AAS Guidance and Control Conference*, Breckenridge, CO, 2009.
- ¹¹ B. Williams, et al., “Navigation Strategy and Results for New Horizons’ Approach and Flyby of the Pluto System.” *AAS Guidance and Control Conference*, Breckenridge, CO, 2015.